


 Cite this: *RSC Adv.*, 2024, 14, 539

Electrical transport properties of [(1 – x) succinonitrile:xpoly(ethylene oxide)]–LiCF₃SO₃–Co[tris-(2,2′-bipyridine)]₃(TFSI)₂–Co[tris-(2,2′-bipyridine)]₃(TFSI)₃ solid redox mediators†

 Ravindra Kumar Gupta,^{id}*^a Hamid Shaikh,^b Ahamad Imran,^a Idriss Bedja,^c Abrar Fahad Ajaj,^d Abdullah Saleh Aldwayyan,^{de} Aslam Khan^{ib}^a and Rashid Ayub^f

A solid redox mediator (solid electrolyte) with an electrical conductivity ($\sigma_{25^\circ\text{C}}$) greater than 10^{-4} S cm⁻¹ is an essential requirement for a dye-sensitized solar cell in the harsh weather of Gulf countries. This paper reports the electrical properties of solid redox mediators prepared using highly dissociable ionic salts: Co[tris-(2,2′-bipyridine)]₃(TFSI)₂, Co[tris-(2,2′-bipyridine)]₃(TFSI)₃, and LiCF₃SO₃ as a source of Co²⁺, Co³⁺, and Li⁺ ions, respectively, in a solid matrix: [(1 – x)succinonitrile:xpoly(ethylene oxide)], where $x = 0, 0.5$, and 1 in weight fraction. In the presence of large size of cations (Co²⁺ and Co³⁺) and large-sized and weakly-coordinated anions (TFSI⁻ and CF₃SO₃⁻), only the succinonitrile–poly(ethylene oxide) blend ($x = 0.5$) resulted in highly conductive amorphous regions with $\sigma_{25^\circ\text{C}}$ of 4.7×10^{-4} S cm⁻¹ for EO/Li⁺ = 108.4 and 3.1×10^{-4} S cm⁻¹ for EO/Li⁺ = 216.8. These values are slightly lower than 1.5×10^{-3} S cm⁻¹ for $x = 0$ and higher than 6.3×10^{-7} S cm⁻¹ for $x = 1$. Only blend-based electrolytes exhibited a downward curve in the $\log \sigma-T^{-1}$ plot, a low value of pseudo-activation energy (0.06 eV), a high degree of transparency, and high thermal stability, making it useful for device applications.

 Received 26th October 2023
 Accepted 13th December 2023

DOI: 10.1039/d3ra07314a

rsc.li/rsc-advances

Introduction

The dye-sensitized solar cell (DSSC) is a third-generation solar cell. The DSSC was presented by O'Regan and Gratzel in 1991 using components such as mesoporous and nanostructured n-type semiconducting transparent oxide, TiO₂ layer on a fluorine-doped tin oxide (FTO) glass as a working electrode (WE), ruthenium-based dye for light absorption and electron injection into TiO₂, I⁻/I₃⁻ redox couple-based liquid redox mediator, and platinized FTO glass as a counter electrode (CE).¹ The liquid redox mediator consisted of tetrapropyl ammonium iodide, KI,

and iodine in a mixture of ethylene carbonate and acetonitrile (ACN) to regenerate the dye at the dye–TiO₂–electrolyte interface, inhibit unwanted back-electron transfer, and regenerate iodide at the CE–electrolyte interface. To date, the highest power conversion efficiency (η), ~11.9% at 100 mW cm⁻², has been achieved for a liquid electrolyte: dimethylpropylimidazolium iodide, I₂, LiI, and 4-*tert*-butylpyridine in acetonitrile with a ruthenium-based dye, and it was commercialized by Sharp.^{2,3}

The I⁻/I₃⁻ redox mediator is unsuitable for long-term utility. The iodine shows sublimation, corrosiveness, dissolution of several interconnects and sealants, and visible light absorption, though, partially at ≈ 430 nm.^{4–20} To avoid these drawbacks, researchers are looking for fast ion-conducting electrolytes with alternative redox couples.^{4–20} The metal complex-based liquid/gel redox mediators offered promising cell efficiency at one sun with various dyes. For example, Cu⁺/Cu²⁺ redox mediators exhibited η as high as 12.5% for HY64 dye and 13.1% for Y123 + XY1 dyes.^{18,19} A Co²⁺/Co³⁺ redox mediator had η of 13.6% with ZL003 dye.²¹ The utilization of ionic liquids with ACN led to η of 14.3% with ADEKA-1 + LEG4 dyes.²² The jellification in an inorganic^{23,24} and organic^{25,26} frameworks led to promising efficiency at the partial sun value.

Unfortunately, these redox mediators are in either a liquid or a gel state. The liquid nature of the electrolyte in the DSSCs is known to create internal pressure at the high operational temperature (50–80 °C) of Gulf regions, thereby breaking up the

^aKing Abdullah Institute for Nanotechnology, King Saud University, Riyadh 11451, Saudi Arabia. E-mail: rgupta@ksu.edu.sa; aimran@ksu.edu.sa; aslamkhan@ksu.edu.sa

^bSABIC Polymer Research Centre, College of Engineering, King Saud University, Riyadh 11421, Saudi Arabia. E-mail: ham-shaikh@ksu.edu.sa

^cCornea Research Chair, Department of Optometry, College of Applied Medical Sciences, King Saud University, Riyadh 11433, Saudi Arabia. E-mail: bedja@ksu.edu.sa

^dDepartment of Physics and Astronomy, College of Science, King Saud University, Riyadh 11451, Saudi Arabia. E-mail: dwayyan@ksu.edu.sa

^eK.A. CARE Energy Research and Innovation Centre, King Saud University, Riyadh, Saudi Arabia

^fDepartment of Science, Technology and Innovation Unit, King Saud University, Riyadh 11451, Saudi Arabia. E-mail: rayub@ksu.edu.sa

† Electronic supplementary information (ESI) available. See DOI: <https://doi.org/10.1039/d3ra07314a>



device and causing solvent leakage. Though this problem is solvable by hermetic sealing, the DSSC fabrication becomes non-scale-up.^{6,8,12} This shows a requirement to replace a liquid or gel redox mediator with a solid one. The solid nature of the mediators makes the device compact, safe, and lightweight. Therefore, we started to develop solid redox mediators as a substitute for the commercially available silicon-based solar cells. Silicon-based solar cells are known to exhibit a lower η in high-temperature and desert regions.³

Recently, we reported the first solid $\text{Co}^{2+}/\text{Co}^{3+}$ redox mediators with $[(1-x)\text{succinonitrile}:x\text{poly(ethylene oxide)}]$ as a solid matrix, LiTFSI as a source of Li^+ ions, and $\text{Co}[\text{tris-(2,2'-bipyridine)}]_3(\text{TFSI})_2/\text{Co}[\text{tris-(2,2'-bipyridine)}]_3(\text{TFSI})_3$ as a source of $\text{Co}^{2+}/\text{Co}^{3+}$ ions.²⁷ These were based on the optimized ACN-based liquid redox mediator.¹¹ In these mediators, tris-(2,2'-bipyridine) abbreviated as bpy, is a ligand binding to the cobalt ion. The anion, TFSI⁻ standing for bis(trifluoromethyl)sulfonylimide, or $(\text{CF}_3\text{SO}_2)_2\text{N}^-$, has lower values of lattice energy, donor number, and ionic mobility; higher values of molecular weight and dissociation constant; and large ionic size (0.79 nm).^{28,29} We replaced ACN with either succinonitrile (abbreviated as SN; $x = 0$ in weight fraction) or poly(ethylene oxide) (abbreviated as PEO; $x = 1$), or (SN-PEO) blend ($x = 0.5$). A plastic crystal succinonitrile is an excellent matrix/solid solvent because of its low molecular weight, low melting temperature (T_m), high dielectric constant (ϵ), ion transport through the nitrile group, and waxy nature.³⁰⁻³⁵ PEO is the best choice amongst solid polymer matrices because of its eco-friendliness, high thermal stability, the dissociation of ionic salt, solvation of the cations, the segmental chain movement, and the availability of ethereal oxygen for ion transport.^{36,37} The redox mediators exhibited electrical conductivity ($\sigma_{25^\circ\text{C}}$) of $2.1 \times 10^{-3} \text{ S cm}^{-1}$ for $x = 0$ and $9.7 \times 10^{-7} \text{ S cm}^{-1}$ for $x = 1$.²⁷ The (SN-PEO) blend-based redox mediator ($x = 0.5$) achieved $\sigma_{25^\circ\text{C}}$ of $7.2 \times 10^{-4} \text{ S cm}^{-1}$, close to that of the redox mediator with $x = 0$. This redox mediator only had a downward curve in the $\log-T^{-1}$ plot, a low pseudo-activation energy value, a high transparency level in a wide wavelength range, and high thermal stability. We observed that an SN-PEO-ions interaction, the large size of Co^{2+} (0.13 nm) and Co^{3+} (0.11 nm) ions, and the plasticizing properties of TFSI⁻ ions and succinonitrile are responsible for a complete arrest of the highly conductive amorphous phase, thereby the higher $\sigma_{25^\circ\text{C}}$ -value.

To establish the above findings, we selected another lithium salt, LiCF_3SO_3 , in place of LiTFSI in series and prepared $[(1-x)\text{SN}:x\text{PEO}]-\text{LiCF}_3\text{SO}_3-\text{Co}[\text{tris-(2,2'-bipyridine)}]_3(\text{TFSI})_2-\text{Co}[\text{tris-(2,2'-bipyridine)}]_3(\text{TFSI})_3$ redox mediators identically. The electrical transport properties are presented in the paper for the first time, and the results are noted as comparable. Trifluoromethane sulfonate, or CF_3SO_3^- is generally shortened to Tf or triflate. As compared with TFSI⁻ ion, CF_3SO_3^- ion has slightly lower values of ionic size (0.44 nm), molecular weight, dissociation constant, and ionic conductivity. However, it has similar levels of dissociability, thermal stability, and electrochemical stability. Additionally, the CF_3SO_3^- ion has higher values for ionic mobility and donor number.^{28,29} The solid redox mediators with $x = 0, 0.5$ (EO/Li⁺ = 108.4 and 216.8), and 1 (EO/Li⁺ =

216.8) are hereafter referred to as SNE, Blend 1E, Blend 2E, and PEOE, respectively, indicating the matrix (SN, Blend, or PEO) with an extension E for electrolyte. We also synthesized a liquid redox mediator (ACNE) using acetonitrile to compare the electrical transport properties.¹¹ We used impedance spectroscopy with different temperatures to determine the electrical conductivity of solid and liquid redox mediators to know their nature and activation energy. Many common methods, including XRD, FT-IR spectroscopy, UV-visible spectroscopy (UV-vis), polarized optical microscopy (POM), SEM, and DSC, were used to find plausible explanations of electrical transport properties. Thermogravimetric analysis (TGA) assessed the thermal stability of the solid electrolytes.

Results and discussion

Table 1 shows an average value of $\sigma_{25^\circ\text{C}}$ with standard deviation (SD) for SNE, Blends 1E & 2E, PEOE, and ACNE redox mediators. The ACNE possessed $\sigma_{25^\circ\text{C}}$ of $1.6 \times 10^{-2} \text{ S cm}^{-1}$. Many liquid electrolytes²⁷⁻²⁹ also have a similar $\sigma_{25^\circ\text{C}}$ -value. It is a known fact that acetonitrile is a liquid at room temperature and acts as a polar aprotic organic solvent with $\epsilon \approx 36.6$, molar enthalpy (ΔH) $\approx 40.6 \text{ kJ mol}^{-1}$, donor number (DN) $\approx 14.1 \text{ kcal mol}^{-1}$, and acceptor number ≈ 18.9 .^{38,39} The FT-IR spectroscopy as discussed later showed that the ACN assisted in breaking apart the ionic salts with a huge number of free ions. The free cations moved through nitrile groups of the ACN and resulted in $\sigma_{25^\circ\text{C}} \approx 10^{-2} \text{ S cm}^{-1}$. The SNE exhibited $\sigma_{25^\circ\text{C}} \approx 1.5 \times 10^{-3} \text{ S cm}^{-1}$, which is akin to the previously reported SN-based solid electrolytes.^{27,30-35} Succinonitrile is a non-ionic organic solid solvent with $\epsilon \approx 55$, $\Delta H \approx 139.7 \text{ kJ mol}^{-1}$, and DN $\approx 14 \text{ kcal mol}^{-1}$ at 25°C . It melts at $\sim 58^\circ\text{C}$ with an ϵ value of 62.6.^{30,39} This means that, like acetonitrile, SN helped to dissociate ionic salts, leaving free ions for transport. The SNE has $\sigma_{25^\circ\text{C}}$ -value an order of magnitude less than the ACNE. This decrease in $\sigma_{25^\circ\text{C}}$ is because of the solid nature of the succinonitrile, as indicated by the $\log \sigma$ vs. T^{-1} study and discussed later.

The PEOE exhibited $\sigma_{25^\circ\text{C}}$ value, $6.3 \times 10^{-7} \text{ S cm}^{-1}$, which is nearly four orders of magnitude higher than the highly crystalline PEO. This conductivity enhancement is because the PEO has many good qualities, including the ability to break apart ionic salt ($\epsilon \approx 5-8$ and DN $\approx 22 \text{ kcal mol}^{-1}$), ethereal oxygen-based ion transport, and cation solvation through a proper spacing between successive ethereal oxygen.³⁶ This is also

Table 1 Electrical transport parameters of SNE, Blends 1E & 2E, PEOE, and ACNE. (I) and (II) Stand for temperature regions. Please see the text for details

Electrolytes	$\sigma_{25^\circ\text{C}}$ (S cm^{-1}) [SD]	E_a (eV)
ACNE	1.65×10^{-2} [2.2×10^{-3}]	0.16
SNE ($x = 0$)	1.5×10^{-3} [7.8×10^{-5}]	0.77 (I), 0.13 (II)
Blend 1E ($x = 0.5$)	4.7×10^{-4} [3.5×10^{-5}]	0.06
Blend 2E ($x = 0.5$)	3.1×10^{-4} [4.0×10^{-5}]	0.06
PEOE ($x = 1$)	6.3×10^{-7} [2.6×10^{-7}]	1.22 (I), 0.44 (II)

helped by the large size of the ions serving as plasticizers.^{40,41} However, the low $\sigma_{25^\circ\text{C}}$ value suggests the dominance of the crystalline phase of the PEO, as pointed out by the XRD, UV-vis, POM, SEM, and DSC studies.^{29,36,37}

Blend 1E achieved $\sigma_{25^\circ\text{C}} \approx 4.7 \times 10^{-4} \text{ S cm}^{-1}$ and Blend 2E possessed $\sigma_{25^\circ\text{C}} \approx 3.1 \times 10^{-4} \text{ S cm}^{-1}$. Both had $\sigma_{25^\circ\text{C}}$ -values closer to the SNE than the PEOE, indicating the plasticizing effect of the succinonitrile.^{42–45} Additionally, more free ions are available for migration as a result of the race between nitrile and ethereal oxygen to bind a cation.^{43–46} One can also note that the Blend 1E has a slightly higher $\sigma_{25^\circ\text{C}}$ -value than the Blend 2E. The results of FT-IR spectroscopy, UV-vis, SEM, and DSC investigations, as elaborated later, suggest that more free ions and amorphous regions for the former may be the causes of the higher $\sigma_{25^\circ\text{C}}$ -value.

Fig. 1 depicts $\log \sigma$ vs. T^{-1} plots of ACNE, SNE, Blends 1E & 2E, and PEOE redox mediators. This figure showed regions (I) and (II) for the solid-state and liquid/amorphous phases of SNE and PEOE, respectively. The ACNE, SNE, and PEOE demonstrated a consistent decline in the $\log \sigma$ as T^{-1} increased. The redox mediators produced analogously using LiTFSI had an identical linear trend.²⁷ This trend indicates homogeneous electrolytes, where ion movement in a solid or liquid medium is thermally activated. This thermally activated behavior follows an Arrhenius equation, $\sigma = \sigma_0 \exp[-E_a/k_B T]$.^{34,36,37} This expression had notations σ_0 , E_a , and k_B with their usual meanings: pre-exponential factor, activation energy, and the Boltzmann constant, respectively. The activation energy obtained from the slope of the linear curve is displayed in Table 1 for comparison. ACNE had $E_a \approx 0.16 \text{ eV}$. In regions (I) and (II), SNE had E_a of 0.77 and 0.13 eV, respectively. PEOE displayed $E_a \approx 1.22$ and 0.44 eV in regions (I) and (II), respectively. SNE and PEOE possessed $E_a > 0.3 \text{ eV}$, making them inapplicable for a device application.⁴⁷

Blends 1E & 2E illustrated the movement of segmental chains and the semi-random movement of small polymeric chains in amorphous domains through the downward $\log \sigma$ vs.

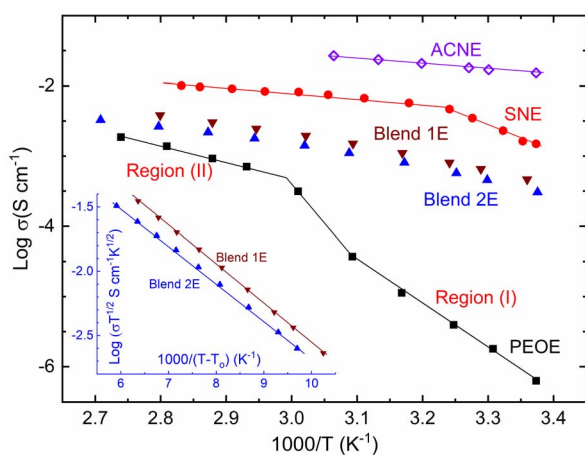


Fig. 1 $\log \sigma - T^{-1}$ plots of ACNE, SNE, Blends 1E & 2E, and PEOE. Inset showed $\log \sigma T^{1/2} - (T - T_0)^{-1}$ plots for Blends 1E & 2E. Please see the text for details of regions (I) and (II).

T^{-1} curves.^{12,29,36,37} The amorphous domain has a characteristic temperature, T_0 , the ideal vitreous transition temperature. Vogel-Tammann-Fulcher (VTF) used T_0 in their empirical relation, $\sigma = \sigma_0 T^{-1/2} \exp[-B/k_B(T - T_0)]$ to portray the downward curve. This relation had a notation B for the pseudo-activation energy. The inset of Fig. 1 shows the $\log \sigma T^{1/2}$ vs. $(T - T_0)^{-1}$ plot for Blends 1E & 2E. This plot demonstrated a linear trend for both mediators. Blends 1E & 2E had a similar slope value and, thereby, the B -value ($\approx 0.06 \text{ eV}$). The B -value is comparable to those obtained for the PEO-SN blend-based Γ^-/I_3^- and $\text{Co}^{2+}/\text{Co}^{3+}$ redox mediators.^{27,44,45} This indicates easy ion transport as in liquid electrolytes. Also, Blends 1E & 2E possessed a B -value $< 0.3 \text{ eV}$, a requirement for DSSC application.

Fig. 2 exhibits XRD curves of SNE, Blends 1E & 2E, and PEOE. SNE and PEOE showed XRD patterns resembling those of the matrix, SN, and PEO, respectively, though the reflection peaks were relatively weak and broad.^{42,44} This indicates a disorder in molecules of succinonitrile and polymeric chains of poly(ethylene oxide) induced by the large size of ions.^{34,36,42,44,45} Furthermore, the lack of distinctive peaks of the ionic salts in the XRD profiles of SNE and PEOE suggested a complete dissociation of the salts. The XRD profiles of Blends 1E & 2E possessed none of the distinctive peaks of the constituents. The lack of peaks indicated the complete amorphous phase formation, as observed earlier for the (PEO-SN)-MI-I₂ and (PEO-SN)-LiX solid electrolytes, where M = Li and K, and X = TFSI and ClO₄.^{44,45,48–50} The absence of peaks is due to an interaction between succinonitrile molecules, poly(ethylene oxide) chains, and ions.^{49,50} One can also note a difference in hump position with a 2θ -value higher for the more conductive electrolyte (Blend 1E), as observed earlier for a similar system.²⁷ This is probably due to a better solvation of the ions with the $\text{CH}_2\text{-CH}_2\text{-O}$ chains of the PEO in the presence of succinonitrile molecules, resulting in more amorphicity for the Blend 1E. The findings were supported by FT-IR spectroscopy, UV-vis, POM, SEM, and DSC investigations.

Fig. 3 exhibits FT-IR spectra of SNE, Blends 1E & 2E, PEOE, and ACNE redox mediators, along with the cobalt and lithium salts in fingerprint, $\nu_{\text{C}\equiv\text{N}}$, and $\nu_{\text{C-H}}$ regions for comparison.

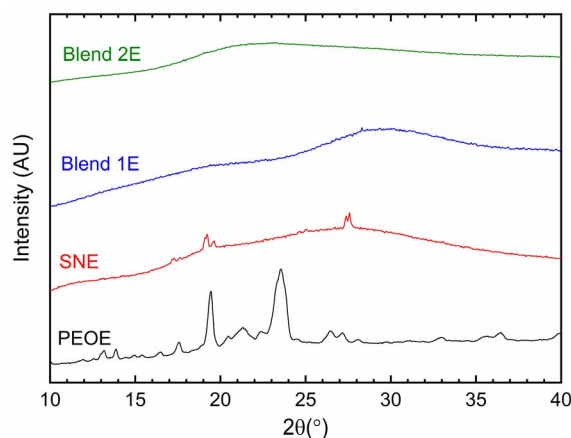


Fig. 2 XRD curves of SNE, Blends 1E & 2E, and PEOE.

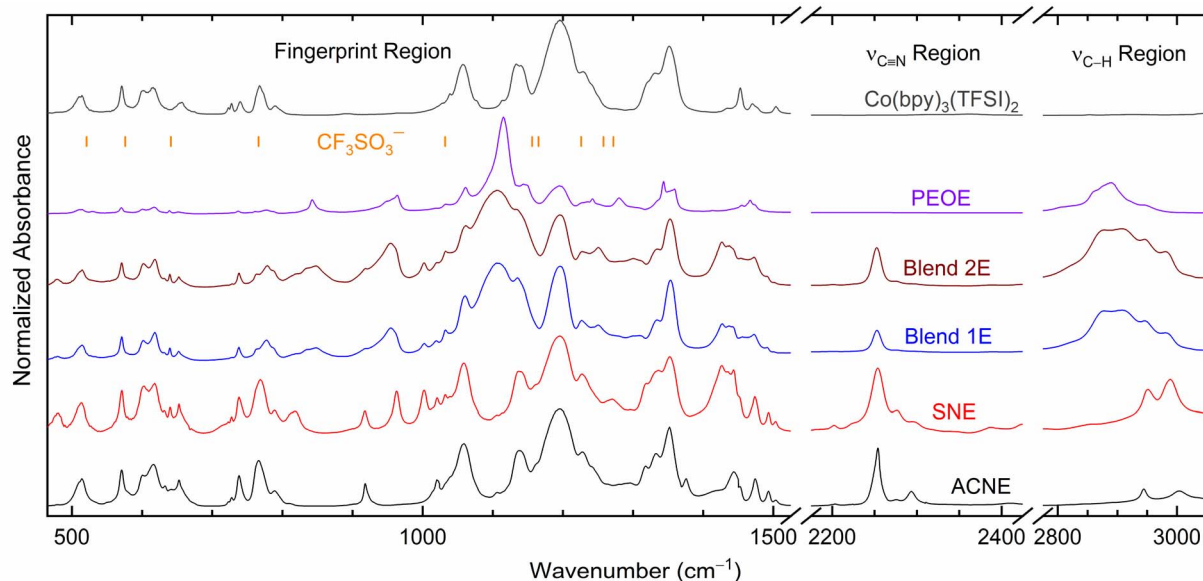


Fig. 3 FT-IR spectra of ACNE, SNE, Blends 1E & 2E, and PEOE, including $\text{Co}(\text{bpy})_3(\text{TFSI})_2$ salt. Vertical lines, CF_3SO_3^- ions.

Table S1† presented the vibrational frequencies and their assignments for redox mediators, acetonitrile,⁵¹ succinonitrile,^{42,44,45,52} PEO,^{42,44,45,53} succinonitrile-PEO blend,^{42,44,45} LiCF_3SO_3 ,⁵⁴⁻⁵⁶ and $\text{Co}(\text{bpy})_3(\text{TFSI})_2$.^{48,57-59} Bernson and Lindgren⁵⁴ observed the presence of CF_3SO_3^- ions *via* $\nu_{\text{s,SO}_3}$ mode at 1032 cm^{-1} (free ions) and 1040 cm^{-1} (coordinated ions), $\nu_{\text{a,CF}_3}$ mode at 1156 cm^{-1} (free) and 1165 cm^{-1} (coordinated), $\nu_{\text{s,CF}_3}$ mode at 1226 cm^{-1} (free), $\nu_{\text{a,SO}_3}$ mode at 1258 cm^{-1} (coordinated), 1272 cm^{-1} (free), and 1300 cm^{-1} (coordinated) for the 0.05 M LiCF_3SO_3 solution in acetonitrile. Rhodes and Frech⁵⁶ observed the $\delta_{\text{a,SO}_3}$ mode at 521 and 576 cm^{-1} , $\delta_{\text{a,CF}_3}$ mode at 582 and 588 cm^{-1} , $\delta_{\text{s,SO}_3}$ mode at 641 cm^{-1} , $\delta_{\text{s,CF}_3}$ mode at 761 and 766 cm^{-1} , and $\nu_{\text{s,SO}_3}$ mode at 1044 cm^{-1} in the infrared spectrum of the $\text{PEO}_3\text{LiCF}_3\text{SO}_3$ polymer electrolyte through a symmetry-based analysis. The position and intensity of a mode were dependent on salt concentration because of the formation of free and coordinated ions. The same was observed for the poly(propylene oxide)- LiCF_3SO_3 polymer electrolyte.^{54,55} Though the formation of coordinated ions decreases the number of free ions, this results in increasing the mobility in the polar polymer, reducing the solvent-salt interaction, and, thereby increasing the amorphicity in the electrolyte.⁵⁸ In the present case, the CF_3SO_3^- modes have overlapped with those of the relatively stronger TFSI^- modes because of the higher concentration of TFSI^- , making extraction of any information regarding the matrix- CF_3SO_3^- interaction difficult. The observed matrix- TFSI^- interaction in the fingerprint, $\nu_{\text{C}\equiv\text{N}}$, and $\nu_{\text{C-H}}$ regions has been discussed below. It is noteworthy that the strongly solvated free and unpaired TFSI^- ion results in peaks at 1057 , 1133 , 1196 , and 1351 cm^{-1} ; whereas the coordinated TFSI^- ion produces peaks at 1229 and 1331 cm^{-1} .^{48,58,59}

ACNE observed an insignificant change in the position of the modes of the TFSI^- ion and bpy ligand, indicating a complete dissociation of ionic salts by the ACN, resulting in a vast

number of free ions. The ACNE spectrum also showed weak coordinated peaks at 1229 and 1331 cm^{-1} as shoulders, indicating the presence of a few ion pairs. Thus, ACNE had many free ions for transport, resulting in $\sigma_{25^\circ\text{C}} \approx 10^{-2}\text{ S cm}^{-1}$.

SNE showed the spectrum comprising modes of the constituents without a substantial alter in the position in all regions except for the bpy ring position at 1443 (1453 cm^{-1}) and 1474 (1470 cm^{-1}). Like the ACNE, the SNE showed weak coordinated TFSI^- peaks as shoulders. These observations reveal a complete dissociation of ionic salts by the SN in SNE, thereby creating many free ions for transport along with a few ion pairs. However, the succinonitrile-bpy interaction hinders the ion transport, resulting in $\sigma_{25^\circ\text{C}} \approx 10^{-3}\text{ S cm}^{-1}$.

PEOE demonstrated the PEO-salt interaction through a shift in the position of several modes in the fingerprint region only. The changes were at 651 (656 cm^{-1} , $\delta_{\text{a,SO}_3}$), 737 (740 cm^{-1} , $\nu_{\text{s,SNS}}$), 777 (767 cm^{-1} , bpy ring), 1115 (1109 cm^{-1} , $\nu_{\text{s,COC}}$), 1144 (1133 cm^{-1} , $\nu_{\text{s,SO}_2}$; 1149 cm^{-1} , ν_{CC}), and 1343 (1351 cm^{-1} , $\nu_{\text{a,SO}_2}$). This interaction most probably hindered the transport of ions, resulting in poor $\sigma_{25^\circ\text{C}}$ -value, $6.3 \times 10^{-7}\text{ S cm}^{-1}$. The spectrum of the PEOE also showed a very sharp $\nu_{\text{s,COC}}$ mode at 1115 cm^{-1} with two shoulder peaks, $\nu_{\text{a,COC}}$ mode at 1061 cm^{-1} and ν_{CC} mode at 1144 cm^{-1} , revealing the crystalline nature of the PEOE.^{42,44,45,53}

Blends 1E & 2E demonstrated their amorphous nature by displaying a broad $\nu_{\text{s,COC}}$ mode at 1106 cm^{-1} with a weak shoulder peak of the $\nu_{\text{a,COC}}$ mode at 1061 cm^{-1} . Similar to SNE, the blend-bpy ring interaction can be visualized in the fingerprint region at 777 cm^{-1} (762 cm^{-1} , δ_{CH_2} ; 767 cm^{-1} , bpy-ring), 1437 (1453 cm^{-1} , δ_{CH_2} and bpy ring), and 1473 (1469 cm^{-1} , δ_{CH_2} and bpy ring), indicating the prominent role of succinonitrile in the interaction with the bpy ring. The blend-salt interaction also resulted in a blueshift in the ν_{CH_2} modes in the region, 2800 – 3100 cm^{-1} , and ion pairing peaks at ~ 1227 and

$\sim 1334\text{ cm}^{-1}$. As mentioned earlier, this shift is due to an increase in amorphicity.^{42,44,45,53} The Blend 1E observed marginally higher blueshift than the Blend 2E.

Fig. 4 demonstrates the solvent/matrix-salt interaction effect on intensity for the fingerprint region.²⁷ This figure showed relative intensities $\Delta I_1 = I_{919\text{ cm}^{-1}}/I_{1196\text{ cm}^{-1}}$ and $\Delta I_2 = I_{1105\text{ cm}^{-1}}/I_{1196\text{ cm}^{-1}}$ for redox mediators, where I stands for intensity at 919 cm^{-1} for $\nu_{\text{s,C-CN}}$ mode of acetonitrile/succinonitrile; at 1105 cm^{-1} for $\nu_{\text{s,COC}}$ mode of PEO; and at $\sim 1196\text{ cm}^{-1}$ for the $\nu_{\text{a,CF}_3}$ mode of ionic salts. The $I_{919\text{ cm}^{-1}}$ had the trend of PEOE (=0) \ll Blend 1E < Blend 2E < SNE \approx ACNE. The $I_{1196\text{ cm}^{-1}}$ had the trend: PEOE \ll Blend 2E < Blend 1E \approx SNE \approx ACNE. These resulted in ΔI_1 with a trend: PEOE (=0) \ll Blend 1E \ll Blend 2E \approx SNE \approx ACNE. As observed earlier, the high value of ΔI_1 indicates a low level of nitrile-salt interaction. Also, $\Delta I_1(\text{Blend 2E}) \approx 2 \times \Delta I_1(\text{Blend 1E})$, revealing a role of concentration of salt because $\text{EO/Li}^+(\text{Blend 2E}) = 2 \times \text{EO/Li}^+(\text{Blend 1E})$. Thus, the higher salt concentration of Blend 1E led to more ion pairs, thereby higher polymeric flexibility and amorphicity. The ΔI_2 provided a similar statement, too. The $I_{1105\text{ cm}^{-1}}$ had the following trend: PEOE (=1) = Blend 2E = Blend 1E \gg SNE = ACNE (=0), which resulted in ΔI_2 with a trend: PEOE \gg Blend 2E > Blend 1E \gg SNE = ACNE (=0). This trend revealed that the interaction between PEO and salt, thereby PEO crystallinity, is low for the Blends 1E & 2E, and high for the PEOE. The UV-vis, POM, and SEM studies, which have been covered below, corroborate these results.

Fig. 5 shows the transmittance spectra of ACNE, SNE (liquid and solid), Blends 1E & 2E, and PEOE. The transmittance values at 350 nm (UV-A region) and 555 nm (visible region) are as follows. UV-A region: $\sim 3.3\%$ (ACNE), 0.5% (SNE_liquid), 0% (SNE_solid), 66.6% (Blend 1E), 68.8% (Blend 2E), and 45.4% (PEOE). Visible region: $\sim 99.9\%$ (ACNE), 99.5% (SNE_liquid), 15.1% (SNE_solid), 99% (Blend 1E), 91.8% (Blend 2E), and 71.9% (PEOE). The transparency of the PEO-based electrolytes demonstrated the order as Blend 1E > Blend 2E \gg PEOE. As discussed later, this is due to the level of PEO crystallinity, which is the lowest for Blend 1E and the highest for PEOE.⁴⁵ It is important to mention that only Blend 1E demonstrated

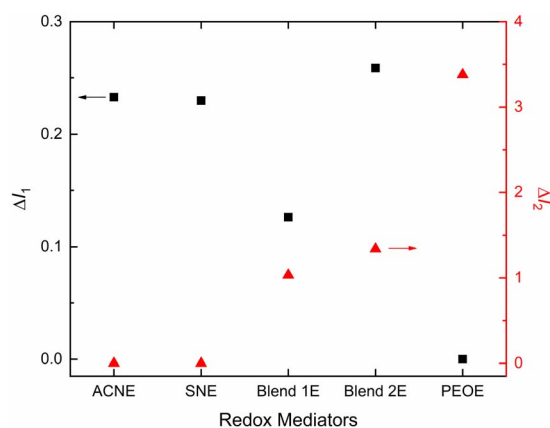


Fig. 4 Relative intensities: ΔI_1 and ΔI_2 of ACNE, SNE, Blends 1E & 2E, and PEOE.

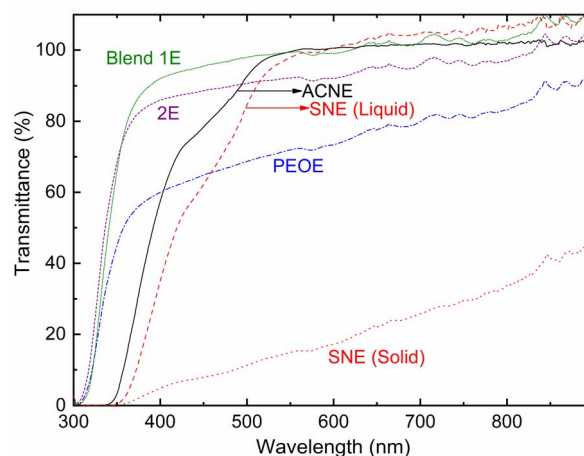


Fig. 5 Transmittance spectra of ACNE, SNE (liquid and solid), Blends 1E & 2E, and PEOE.

a significant level of transparency across all wavelengths, suggesting its possible suitability for use in the device. These results corroborate the POM results discussed below.

Fig. 6 portrays POM images of the PEO-based redox mediators: PEOE, Blend 1E, and Blend 2E. The image of the PEOE showed diamond-like spherulites as well as dark regions. Short, randomly oriented PEO chains result in the former, while the amorphous domain accounts for the latter.^{44,45} The abundance of spherulites in the amorphous regions indicates a high degree of crystallinity in PEO, which is the key factor contributing to the poor electrical conductivity of PEOE. The Blends 1E & 2E did not show any spherulite, indicating the arrest of the amorphous phase.

Fig. 7 shows SEM images of mesoporous TiO_2 film filled with a solid redox mediator (SNE, Blends 1E & 2E, and PEOE) and an image of a bare mesoporous TiO_2 film as an inset for direct

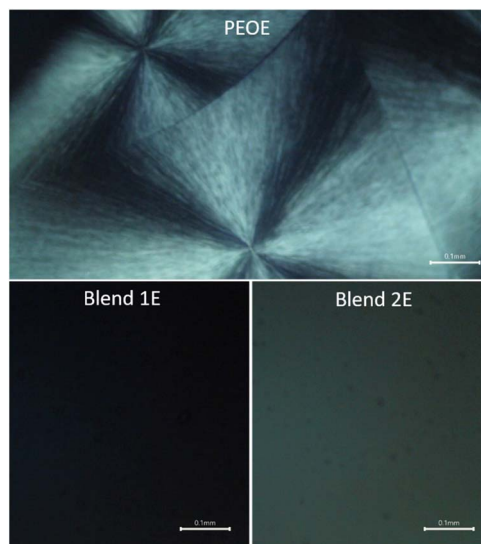


Fig. 6 POM images of PEO-based redox mediators: PEOE, Blend 1E, and Blend 2E. Scale bar: 0.1 mm.

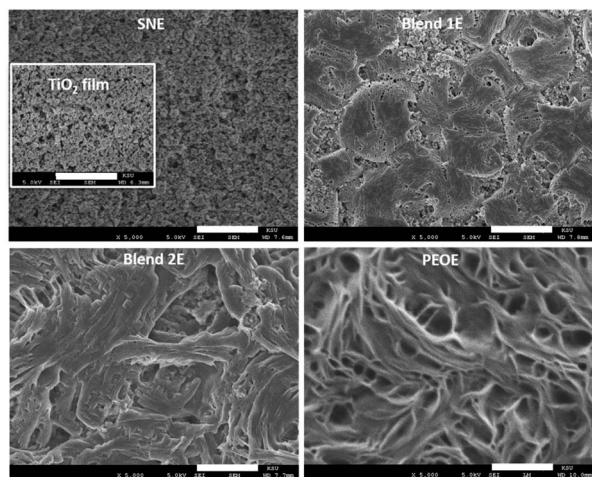


Fig. 7 SEM images of SNE, Blends 1E & 2E, and PEOE on mesoporous TiO₂ film (inset). Scale bar: 5 μm.

comparison. Having a solid solvent (succinonitrile), SNE impregnated the nanopores of the TiO₂ film well. The Blend 1E resulted in a smoother surface than the Blend 2E. According to the FT-IR spectroscopy analysis (Fig. 4), Blend 1E shows increased polymeric flexibility and amorphicity because of its elevated salt content, leading to a higher number of ion pairs. The PEOE exhibited a coarse surface characterized by many fibril-like features, suggesting a high concentration of PEO chains. The DSC study corroborates these findings and is addressed below.

Fig. 8 displays DSC curves of SNE, Blends 1E & 2E, and PEOE solid redox mediators. The endothermic peak, corresponding to T_m of the redox mediator, emerged at 41 and 45.8 °C for SNE, 0 and 23.2 °C for Blend 1E, 7.8 and 26 °C for Blend 2E, and 65.2 °C for PEOE. The T_m -value was 58 °C for SN,³⁴ 30 °C for PEO-SN blend,⁴² and 66 °C for PEO,⁴² revealing that the redox mediator had a lower T_m -value than its matrix. The SN-based electrolytes also exhibited weak multiplets. The existence of the multiplet indicates the formation of a solid solution and/or

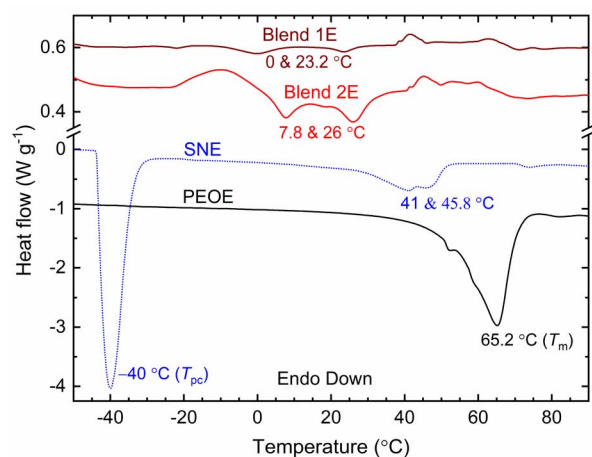


Fig. 8 DSC curves of SNE, Blends 1E & 2E, and PEOE.

a liquid eutectic phase by the SN-salt interaction.³⁰ The multiplet increases the amorphicity. The solid solution and eutectic phase contain free ions, too. We calculated the crystallinity of the PEO-based redox mediators and noted 0.7% for Blend 1E, 2.3% for Blend 2E, and 72.1% for PEOE, controlling the conductivity value Blend 1E > Blend 2E \gg PEOE.^{42–45} The SNE had an endothermic peak at -40 °C, too. This peak is the crystal-to-plastic crystal phase transition temperature (T_{pc}) of the matrix.³⁴ The lack of the T_{pc} peak for the Blends 1E & 2E revealed the blend-salt interaction.^{42–45}

An initial plateau region of the TGA curve corresponds to the thermal stability of a solid.⁴² Fig. 9 shows the TGA curves of the SNE, Blends 1E & 2E, and PEOE, depicting the plateau nearly up to 75, 125, and 200 °C, respectively, and thus their thermal stability. SNE and PEOE portrayed a single-stage decomposition with a massive drop in mass at nearly 125 °C and 300 °C because of the matrix, respectively. Blends 1E & 2E, however, portrayed two-stage degradations because of the SN-PEO blend matrix.²⁷ Because Blend 1E had a higher salt concentration than Blend 2E, the first-stage degradation occurred more slowly for Blend 1E.

Notably, the Co²⁺/Co³⁺ redox couple suffers from mass diffusion problems in DSSCs, resulting in poor η -value.⁶⁰ The mass transport phenomenon in DSSC depends strongly on the porosity of mesoporous TiO₂ film. Following the procedure of Yella *et al.*,⁶⁰ we used 0.06 M TiCl₄ aqueous solution for blocking layer of TiO₂, screen printing of 18NRT paste (TiO₂ particle size 18 nm), and screen printing of Ti-nanoxide R/SP paste (TiO₂ particle size > 100 nm) on 15 Ω □⁻¹ FTO glass for preparing nearly 6 μm mesoporous TiO₂ film after sintering at 500 °C for 30 minutes. The TiO₂ film was sensitized with a 0.2 mM solution of Y123 dye and chenodeoxycholic acid in a tetrahydrofuran-ethanol solvent mixture (1 to 4 volume ratio).⁶⁰ This dye-sensitized TiO₂ layer was infiltrated with a redox mediator and barricaded with a Meltonix (25 μm) film. This layer was covered with a platinum film on the FTO glass. The DSSC was subjected to a J - V study under simulated solar irradiation of 100 mW cm⁻² using a PV measurement (USA) unit. Fig. 10 shows the J - V

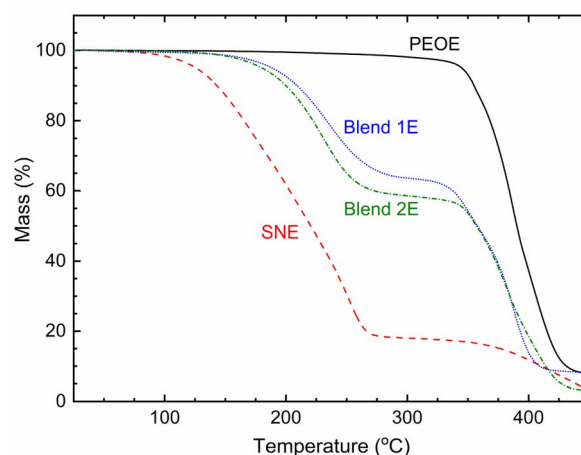


Fig. 9 TGA curves of SNE, Blends 1E & 2E, and PEOE.

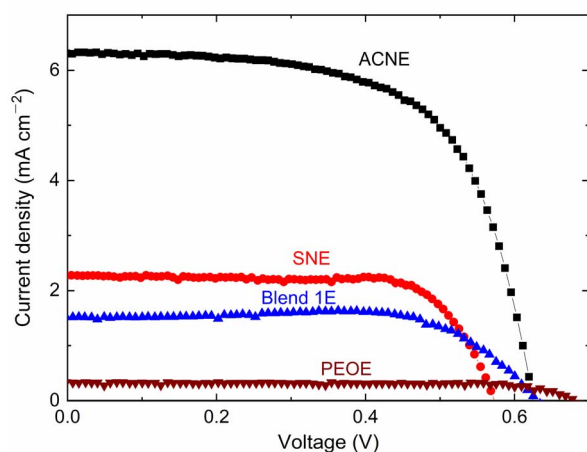


Fig. 10 J - V curves of ACNE, SNE, Blend 1E, and PEOE at 25 °C and one sun.

curves of ACNE, SNE, Blend 1E, and PEOE, which resulted in photovoltaic cell parameters, such as open-circuit voltage (V_{OC}), short-circuit current density (J_{SC}), fill factor (FF), and efficiency (η). Table 2 presented the photovoltaic cell parameters of ACNE, SNE, Blend 1E, and PEOE with η of 2.5, 1, 0.7, and 0.2%, respectively, adopting the $\sigma_{25^\circ\text{C}}$ -value order: ACNE > SNE > Blend 1E > PEOE. Yella *et al.*⁶⁰ achieved $\eta \approx 9.44\%$ with 30 nm-sized TiO_2 particles for a liquid redox mediator similar to ACNE. This shows a requirement of modification in the pore size of mesoporous TiO_2 film by utilizing a larger size of anatase TiO_2 particles.^{60–63}

Experimental

Synthesis

The chemicals, including the solvents used for the present study, are listed in Table S2.† The PEO had a molecular weight of 1 M g mol^{-1} . Table S3† exhibits the composition of redox mediators. The ACNE and SNE solutions were prepared by dissolving 0.1 M LiCF_3SO_3 , 0.25 M $\text{Co}[\text{tris}-(2,2'\text{-bipyridine})]_3(\text{TFSI})_2$, and 0.06 M $\text{Co}[\text{tris}-(2,2'\text{-bipyridine})]_3(\text{TFSI})_3$ in acetonitrile and succinonitrile, respectively.¹¹ The mixture was stirred at 65 °C for 24 h. The solution cast method produced a self-standing film of the PEO-based redox mediators. A viscous and homogeneous polymeric solution was prepared *via* rigorous stirring followed by pouring on a Teflon-based Petri dish and drying at room temperature under nitrogen gas purging to produce a film. We used 20 ml of acetonitrile to

Table 2 Cells parameters of ACNE, SNE, Blend 1E, and PEOE

Electrolyte	V_{OC} (mV)	J_{SC} (mA cm^{-2})	FF (%)	η (%)
ACNE	624.8	6.3	64	2.52
SNE	572.9	2.3	74.2	0.97
Blend 1E	630.2	1.5	73.6	0.7
PEOE	680.3	0.3	79.5	0.18

dissolve the ingredients at 65 °C for 48 h. The film was further dried for 24 h in a vacuum desiccator.

Characterizations

Impedance spectroscopy. A Teflon spacer with a thickness (l) of 0.05 cm and an area (A) of 0.16 cm^{-2} was sandwiched between platinum plates (blocking electrode) in a sample holder.³⁴ The gap between the plates was then filled with the liquid redox mediator. A sample holder with stainless steel plates serving as a blocking electrode was employed for the PEO-based redox mediators.⁴⁴ We applied 20 mV AC voltage across the electrolyte and acquired the Nyquist curve for the frequency range 10^3 –1 Hz using a PalmSens (the Netherlands) impedance analyzer. The model was Palmsens4. The Nyquist curve resulted in bulk resistance (R_b), thereby the electrical conductivity, $\sigma = l/(AR_b)$.²⁷ The temperature-dependent σ measurement provided a linear curve, thereby, the slope and eventually the activation energy.

X-ray diffractometry. The XRD profile of the film was recorded in a range of 10 – 40° with a step of 0.06° at room temperature (25 °C) using a Bruker (Karlsruhe, Germany) X-ray diffractometer. The model was D2 Phaser utilizing the X-ray of the $\text{CuK}\alpha$ line with a wavelength of 1.54184 Å.

Fourier-transform infrared spectroscopy. A film of redox mediator was deposited on the potassium bromide pellet (size 25 mm, thickness 2 mm). This film was subjected to the IR irradiation of 4000 – 400 cm^{-1} with a resolution of 1 cm^{-1} at room temperature (25 °C) through a PerkinElmer (model Spectrum 100, Waltham, USA) FT-IR spectrometer. The EZ-OMNIC software (version 7.2a) was used to analyze the spectrum.

UV-visible spectroscopy. We collected the transmittance spectrum of liquid or solid redox mediator film on a 1.5 cm^2 microscopic glass substrate using a UV-visible spectrometer (model 8453, Agilent, Santa Clara, USA).

Polarized optical microscopy. A polymeric film with a thickness of less than a micron on a 1.5 cm^2 microscopic glass substrate was deposited using a spin coater. This film was subjected to the polarized optical microscopy study using a Zhuzhou (Hunan, China) polarized microscope. The model was ZZCAT. The magnification was $100\times$.

Scanning electron microscopy. A $7 \mu\text{m}$ thick mesoporous TiO_2 film on a microscopic glass was infiltrated with the redox mediator. A JEOL (Tokyo, Japan) scanning electron microscope (model JSM-7600F) was used to image the film.

Differential scanning calorimetry. Nearly 10 mg of solid redox mediator was placed in an aluminum pan, which was then sealed with a cover. The heat flow of the pan was quantified using a Shimadzu (model DSC-60A, Kyoto, Japan) differential scanning calorimeter. The temperature was ramped from -50 to $90 \text{ }^\circ\text{C}$ at $10 \text{ }^\circ\text{C}$ per minute in the N_2 gas environment.

Thermogravimetric analysis. A TGA unit (model DTG-60H, Shimadzu, Kyoto, Japan) was used to record the TGA curve of solid redox mediators through ramping from room temperature to $550 \text{ }^\circ\text{C}$ at $10 \text{ }^\circ\text{C}$ per minute. This measurement was done under the N_2 gas atmosphere.

Photocurrent–voltage (*I*–*V*) study. The BBA small area solar simulator from PV Measurements, Inc., USA was calibrated to provide an intensity equivalent to one sun using a reference solar cell made of silicon. The *I*–*V* characteristics of the DSSC were obtained at 25 °C using a PV measurement data acquisition system (USA).

Conclusions

We produced solid redox mediators by combining [(1 – *x*)SN: *x*PEO], LiCF₃SO₃, and cobalt salts to study their electrical transport capabilities as potential substitutes for the liquid redox mediator (ACNE). The mediators SNE and PEOE, with *x* values of 0 and 1 respectively, showed electrical conductivity of 1.5×10^{-3} and 6.3×10^{-7} S cm⁻¹ at 25 °C. These values are roughly one and four orders of magnitude lower than that of the ACNE ($\sigma_{25^\circ\text{C}} \approx 1.7 \times 10^{-2}$ S cm⁻¹). Both mediators displayed Arrhenius-type characteristics akin to ACNE. The activation energy estimates for SNE and PEOE were 0.77 and 1.22 eV, respectively, which were greater than the 0.16 eV value for ACNE. PEOE showed a significant PEO crystallinity, 72.1%. Blends 1E & 2E exhibited electrical conductivity of 4.7×10^{-4} and 3.1×10^{-4} S cm⁻¹, respectively, which are roughly two orders of magnitude lower than that of the ACNE. Blends 1E & 2E portrayed VTF-type behavior with a pseudo-activation energy of 0.06 V, which is lower than the 0.3 eV threshold needed for a device application. Blends 1E & 2E exhibited PEO crystallinity of 0.7% and 2.3%, respectively, and demonstrated thermal stability up to a temperature of 125 °C. Blend 1E exhibited elevated levels of electrical conductivity and UV-A-visible-near-infrared transmittance, while demonstrating reduced activation energy and PEO crystallinity. The results align with the discoveries made about the LiTFSI-based redox mediators.²⁷ The results also demonstrated that incorporating ionic salts with large cations and anions into a succinonitrile–poly(ethylene oxide) blend is an effective approach for enhancing the electrical, optical, and thermal characteristics of a solid redox mediator for device applications.

Author contributions

Conceptualization, R. K. G. and I. B.; methodology, R. K. G. and I. B.; formal analysis, R. K. G., H. S. and A. K.; investigation, R. K. G., H. S., A. I., A. K., R. A. and A. F. A.; writing—original draft preparation, R. K. G.; writing—review and editing, R. K. G., I. B. and A. S. A.; supervision, R. K. G.; project administration, R. K. G.; funding acquisition, R. K. G., I. B. and A. S. A.

Conflicts of interest

There are no conflicts to declare.

Acknowledgements

The Authors would like to extend their appreciation to the Deputyship for Research and Innovation “Ministry of

Education” in Saudi Arabia for the financial support through the project (number IFKSUOR3-423-2).

Notes and references

- 1 B. O'Regan and M. Gratzel, *Nature*, 1991, **353**, 737–740.
- 2 Y. Chiba, A. Islam, Y. Watanabe, R. Komiya, N. Koide and L. Y. Han, *Jpn. J. Appl. Phys., Part 2*, 2006, **45**, L638–L640.
- 3 M. A. Green, E. D. Dunlop, G. Siefer, M. Yoshita, N. Kopidakis, K. Bothe and X. Hao, *Prog. Photovoltaics*, 2023, **31**, 3–16.
- 4 A. Hagfeldt, G. Boschloo, L. C. Sun, L. Kloo and H. Pettersson, *Chem. Rev.*, 2010, **110**, 6595–6663.
- 5 A. F. Nogueira, C. Longo and M. A. De Paoli, *Coord. Chem. Rev.*, 2004, **248**, 1455–1468.
- 6 B. Li, L. D. Wang, B. N. Kang, P. Wang and Y. Qiu, *Sol. Energy Mater. Sol. Cells*, 2006, **90**, 549–573.
- 7 A. Yella, H. W. Lee, H. N. Tsao, C. Y. Yi, A. K. Chandiran, M. K. Nazeeruddin, E. W. G. Diau, C. Y. Yeh, S. M. Zakeeruddin and M. Gratzel, *Science*, 2011, **334**, 629–634.
- 8 P. K. Singh, R. K. Nagarale, S. P. Pandey, H. W. Rhee and B. Bhattacharya, *Adv. Nat. Sci.: Nanosci. Nanotechnol.*, 2011, **2**, 023002.
- 9 M. K. Wang, C. Gratzel, S. M. Zakeeruddin and M. Gratzel, *Energy Environ. Sci.*, 2012, **5**, 9394–9405.
- 10 J. Y. Cong, X. C. Yang, L. Kloo and L. C. Sun, *Energy Environ. Sci.*, 2012, **5**, 9180–9194.
- 11 S. Mathew, A. Yella, P. Gao, R. Humphry-Baker, B. F. E. Curchod, N. Ashari-Astani, I. Tavernelli, U. Rothlisberger, M. K. Nazeeruddin and M. Gratzel, *Nat. Chem.*, 2014, **6**, 242–247.
- 12 J. H. Wu, Z. Lan, J. M. Lin, M. L. Huang, Y. F. Huang, L. Q. Fan and G. G. Luo, *Chem. Rev.*, 2015, **115**, 2136–2173.
- 13 L. Giribabu, R. Bolligarla and M. Panigrahi, *Chem. Rec.*, 2015, **15**, 760–788.
- 14 F. Bella, S. Galliano, C. Gerbaldi and G. Viscardi, *Energies*, 2016, **9**, 384.
- 15 M. Freitag, J. Teuscher, Y. Saygili, X. Zhang, F. Giordano, P. Liska, J. Hua, S. M. Zakeeruddin, J. E. Moser, M. Gratzel and A. Hagfeldt, *Nat. Photonics*, 2017, **11**, 372–378.
- 16 S. Venkatesan and Y. L. Lee, *Coord. Chem. Rev.*, 2017, **353**, 58–112.
- 17 H. Iftikhar, G. G. Sonai, S. G. Hashmi, A. F. Nogueira and P. D. Lund, *Materials*, 2019, **12**, 1998.
- 18 N. Vlachopoulos, A. Hagfeldt, I. Benesperi, M. Freitag, G. Hashmi, G. B. Jia, R. A. Wahyuono, J. Plentz and B. Dietzek, *Sustainable Energy Fuels*, 2021, **5**, 367–383.
- 19 K. S. Srivishnu, S. Prasanthkumar and L. Giribabu, *Mater. Adv.*, 2021, **2**, 1229–1247.
- 20 M. Kokkonen, P. Talebi, J. Zhou, S. Asgari, S. A. Soomro, F. Elsehrawy, J. Halme, S. Ahmad, A. Hagfeldt and S. G. Hashmi, *J. Mater. Chem. A*, 2021, **9**, 10527–10545.
- 21 L. Zhang, X. C. Yang, W. H. Wang, G. G. Gurzadyan, J. J. Li, X. X. Li, J. C. An, Z. Yu, H. X. Wang, B. Cai, A. Hagfeldt and L. C. Sun, *ACS Energy Lett.*, 2019, **4**, 943–951.

- 22 K. Kakiage, Y. Aoyama, T. Yano, K. Oya, J. Fujisawa and M. Hanaya, *Chem. Commun.*, 2015, **51**, 15894–15897.
- 23 T. Stergiopoulos, M. Bidikoudi, V. Likodimos and P. Falaras, *J. Mater. Chem.*, 2012, **22**, 24430–24438.
- 24 S. Venkatesan, I. P. Liu, L. T. Chen, Y. C. Hou, C. W. Li and Y. L. Lee, *ACS Appl. Mater. Interfaces*, 2016, **8**, 24559–24566.
- 25 S. Venkatesan, I. P. Liu, C. M. T. Shan, H. S. Teng and Y. L. Lee, *Chem. Eng. J.*, 2020, **394**, 124954.
- 26 P. Karthika, S. Ganesan, A. Thomas, T. M. S. Rani and M. Prakash, *Electrochim. Acta*, 2019, **298**, 237–247.
- 27 R. K. Gupta, H. Shaikh, A. Imran, I. Bedja, A. F. Ajaj and A. S. Aldwayyan, *Polymers*, 2022, **14**, 1870.
- 28 R. Younesi, G. M. Veith, P. Johansson, K. Edström and T. Vegge, *Energy Environ. Sci.*, 2015, **8**, 1905–1922.
- 29 A. Arya and A. L. Sharma, *J. Mater. Sci.*, 2020, **55**, 6242–6304.
- 30 P. J. Alarco, Y. Abu-Lebdeh, A. Abouimrane and M. Armand, *Nat. Mater.*, 2004, **3**, 476–481.
- 31 P. Wang, Q. Dai, S. M. Zakeeruddin, M. Forsyth, D. R. MacFarlane and M. Gratzel, *J. Am. Chem. Soc.*, 2004, **126**, 13590–13591.
- 32 Q. Dai, D. R. MacFarlane and M. Forsyth, *Solid State Ionics*, 2006, **177**, 395–401.
- 33 Z. G. Chen, H. Yang, X. H. Li, F. Y. Li, T. Yi and C. H. Huang, *J. Mater. Chem.*, 2007, **17**, 1602–1607.
- 34 R. K. Gupta, I. Bedja, A. Islam and H. Shaikh, *Solid State Ionics*, 2018, **326**, 166–172.
- 35 R. K. Gupta, H. Shaikh and I. Bedja, *ACS Omega*, 2020, **5**, 12346–12354.
- 36 P. G. Bruce and F. M. Gray, in *Solid State Electrochemistry*, ed. P. G. Bruce, Cambridge University Press Cambridge, United Kingdom, 1995, ch. 6, pp. 119–162.
- 37 R. C. Agrawal and G. P. Pandey, *J. Phys. D: Appl. Phys.*, 2008, **41**, 223001.
- 38 C. Reichardt, *Solvents and Solvent Effects in Organic Chemistry*, WILEY-VCH Verlag GmbH & Co. KGaA, Weinheim, 3 edn, 2003, pp. 23–26.
- 39 *CRC Handbook of Chemistry and Physics*, ed. D. R. Lide, CRC Press/Taylor and Francis, Boca Raton, FL, USA, 2009, pp. 3–6.
- 40 B. Bhattacharya, J. Y. Lee, J. Geng, H. T. Jung and J. K. Park, *Langmuir*, 2009, **25**, 3276–3281.
- 41 R. K. Gupta and I. Bedja, *J. Phys. D: Appl. Phys.*, 2017, **50**, 245501.
- 42 R. K. Gupta, H. M. Kim and H. W. Rhee, *J. Phys. D: Appl. Phys.*, 2011, **44**, 205106.
- 43 R. K. Gupta and H. W. Rhee, *Adv. OptoElectron.*, 2011, **2011**, 102932.
- 44 R. K. Gupta and H. W. Rhee, *Electrochim. Acta*, 2012, **76**, 159–164.
- 45 R. K. Gupta and H. W. Rhee, *J. Phys. Chem. B*, 2013, **117**, 7465–7471.
- 46 M. Patel and A. J. Bhattacharyya, *Electrochem. Commun.*, 2008, **10**, 1912–1915.
- 47 R. C. Agrawal and R. K. Gupta, *J. Mater. Sci.*, 1999, **34**, 1131–1162.
- 48 R. K. Gupta and H. W. Rhee, *Bull. Korean Chem. Soc.*, 2017, **38**, 356–363.
- 49 L. Z. Fan, Y. S. Hu, A. J. Bhattacharyya and J. Maier, *Adv. Funct. Mater.*, 2007, **17**, 2800–2807.
- 50 R. J. Yue, Y. H. Niu, Z. G. Wang, J. F. Douglas, X. Q. Zhu and E. Q. Chen, *Polymer*, 2009, **50**, 1288–1296.
- 51 E. L. Pace and L. J. Noe, *J. Chem. Phys.*, 1968, **49**, 5317–5325.
- 52 O. I. Fengler and A. Ruoff, *Spectrochim. Acta, Part A*, 2001, **57**, 105–117.
- 53 T. Yoshihara, H. Tadokoro and S. Murahashi, *J. Chem. Phys.*, 1964, **41**, 2902–2911.
- 54 A. Bernson and J. Lindgren, *Solid State Ionics*, 1993, **60**, 37–41.
- 55 W. Huang, R. Frech and R. A. Wheeler, *J. Phys. Chem.*, 1994, **98**, 100–110.
- 56 C. P. Rhodes and R. Frech, *Solid State Ionics*, 2000, **136–137**, 1131–1137.
- 57 E. Castellucci, L. Angeloni, N. Neto and G. Sbrana, *Chem. Phys.*, 1979, **43**, 365–373.
- 58 S. J. Wen, T. J. Richardson, D. I. Ghantous, K. A. Striebel, P. N. Ross and E. J. Cairns, *J. Electroanal. Chem.*, 1996, **408**, 113–118.
- 59 I. Rey, J. C. Lassègues, J. Grondin and L. Servant, *Electrochim. Acta*, 1998, **43**, 1505–1510.
- 60 A. Yella, S. Mathew, S. Aghazada, P. Comte, M. Gratzel and M. K. Nazeeruddin, *J. Mater. Chem. C*, 2017, **5**, 2833–2843.
- 61 D. Hwang, H. Lee, S. Y. Jang, S. M. Jo, D. Kim, Y. Seo and D. Y. Kim, *ACS Appl. Mater. Interfaces*, 2011, **3**, 2719–2725.
- 62 D. Hwang, D. Y. Kim, S. Y. Jang and D. Kim, *J. Mater. Chem. A*, 2013, **1**, 1228–1238.
- 63 M. Alduraiibi, M. Hezam, B. Al-Ruhaimi, A. M. El-Toni, A. Algarni, M. Abdel-Rahman, W. Qing and A. Aldwayyan, *Nanomaterials*, 2020, **10**, 413.